Геология и геофизика, т. 65, № 10, с. 1474—1494, DOI: 10.15372/GiG2024111, EDN: OPARCS
Поступила в редакцию 29.10.2023, принята в печать 04.02.2024 *Опубликована онлайн: 07.02.2024*

УДК 551.435.627+550.394

КАРТИРОВАНИЕ СЕЙСМООПАСНЫХ РАЙОНОВ ПО ПОДВЕРЖЕННОСТИ ОПОЛЗНЯМ, ОСНОВАННОЕ НА НЕЧЕТКОЙ ЛОГИКЕ (*на примере бассейна Мила, Алжир*)

В. Четтах[1], С. Межоуд[2], М. Бадеш[3], Р. Хаджи[4]

[1]*Laboratory of Geology and Environment, University of Constantine 1, Algeria*

[2]*Laboratory of Materials and Construction Durability (LMDC), University of Constantine 1, Algeria*

[3]*Department of Land Survey, University of Constantine 1, Algeria*

[4]*Laboratory of Applied Research in Engineering Geology, Geotechnics, Water Sciences and Environment, University of Sétif 1, Algeria*

Настоящее исследование посвящено анализу оползней, вызванных умеренным землетрясением (M_w = 4.9) в северо-восточном районе провинции Мила, которое привело к значительному ущербу и экономическим потерям в районе Эль-Херба и городе Грарем-Гуга. Благодаря обширному полевому исследованию был составлен полный список оползней. Для оценки подверженности территории оползням, вызванным сейсмической активностью, была использована модель нечеткой логики на основе ГИС. Модель включает в себя различные входные факторы, такие как литология, угол наклона, нормализованный относительный индекс растительности (NDVI), расстояние от рек и дорог, осадки и сейсмическая опасность, что отображено на карте. В исследовании сравниваются характеристики различных нечетких операторов и значений гаммы и установлено, что использование нечетких гамма-операторов со значением гаммы 0.8 обеспечивает удовлетворительную согласованность между приведенными факторами и распределением оползней. Более того, использование карты сейсмической опасности как причинного фактора повышает точность картирования районов, подверженных оползням. Данное исследование подчеркивает важность модели нечеткой логики в управлении стихийными бедствиями и планировании опытно-конструкторских работ.

Оползни, вызванные землетрясениями, нечеткие операторы, ГИС, сейсмическая опасность, карты восприимчивости, бассейн Мила

FUZZY LOGIC-BASED LANDSLIDE SUSCEPTIBILITY MAPPING IN EARTHQUAKE-PRONE AREAS: A CASE STUDY OF THE MILA BASIN, ALGERIA

W. Chettah, S. Mezhoud, M. Baadeche, R. Hadji

This research focuses on analyzing landslides triggered by a moderate earthquake (M_w = 4.9) in the northeastern region of the Mila province, which resulted in significant damage and economic losses in the El Kherba district and Grarem Gouga city. Through an extensive field-based investigation, a comprehensive inventory of landslides has been compiled. To assess the susceptibility to landslides triggered by seismic activity, a GIS-based fuzzy logic model was employed. The model incorporates various input factors, such as lithology, slope angle, normalized difference vegetation index (NDVI), distance from rivers and roads, precipitation, and seismic hazard, which is shown on a map. The study compares the performance of different fuzzy operators and gamma values and determines that using fuzzy gamma operators with a gamma value of 0.8 yields a satisfactory consistency with the distribution of landslides. Moreover, incorporating the map of seismic hazard as a causative factor enhances the accuracy of landslide susceptibility mapping. This study underscores the utility of the fuzzy logic model in disaster management and the planning of development activities.

Earthquake-triggered landslides, fuzzy operators, GIS, seismic hazard, susceptibility maps, Mila basin

INTRODUCTION

The global phenomenon of landslides poses a significant and multifaceted challenge, resulting in substantial human casualties and economic damage in mountainous regions worldwide (Mezhoud et al., 2017; Razifard et al., 2019; Berkane et al., 2022). Recent statistics highlight the severity of this issue, with landslides affecting approximately 4.8 million people and causing over 18,000 fatalities between 1998 and 2017 (Wallemacq et al., 2018). The monetary toll of landslides reaches billions of US dollars annually on a global scale, but it is worth noting that this estimate might underrepresent the true extent of the problem because of data gaps in many de-

✉e-mail: mezhoud.sami@umc.edu.dz

veloping countries (Grima et al., 2020). Many landslides have a tendency to reactivate during the winter season, which may be a common occurrence in the Mediterranean region but is not necessarily a global phenomenon. They are intricately linked to a range of predisposing factors encompassing geologic, tectonic, hydrologic, and geotechnical aspects as well as other triggering factors, such as human activities and seismic activity (Aicha et al., 2021, 2022). Consequently, efforts to assess landslide susceptibility, hazard, and risk involve a complex fusion of knowledge incorporating various methodologies (Giles and Griffiths, 2020).

The reliability of the resultant maps crucially hinges on factors like data volume and quality, working scale, and the choice of the appropriate modeling methodology (Baral et al., 2021). It is important to note that these different approaches to landslide susceptibility assessment, albeit diverse, are not mutually exclusive. In fact, comparing their results can significantly enhance the understanding of the quality and reliability of each method (Rahali, 2019).

Landslide susceptibility, hazard, and risk maps play a pivotal role in providing scientific support for government responses to land use practices and landslide hazard management (Wang et al., 2020). They are widely regarded as the initial steps toward mitigating landslide hazards (Mertens et al., 2018). A myriad of methods are employed in landslide susceptibility assessment, generally categorized as qualitative or quantitative (Shano et al., 2020). Some of the most commonly used techniques encompass deterministic models (Min and Yoon, 2021), statistical models like logistic regression (Li and Wang, 2019), and the analytical hierarchy process method developed by Saaty (1977), which is widely adopted in landslide susceptibility mapping (Mandal and Mandal, 2018). More recently, innovative methods, such as fuzzy logic (Tsangaratos et al., 2018), artificial neural network models (Ortiz and Martínez-Graña, 2018), and machine learning (Mohan et al., 2021), have gained traction in landslide susceptibility assessment. Among these methods, GIS-based multicriteria decision analysis, grounded in fuzzy logic, stands out as an accurate and widely applied approach, not only for landslides but also for solving geospatial problems globally (Bahrami et al., 2021). This method leverages a range of membership functions supported by monotonically increasing, monotonically decreasing, and symmetric variables, making it a robust choice for landslide hazard analysis and prediction (Tsangaratos et al., 2018; Razifard et al., 2019; Bahrami et al.,, 2021).

This study delves into the intricate world of landslide susceptibility zoning by exploring the efficacy of various fuzzy logic operators. Our research focuses on an area that experienced a moderate earthquake (M_w = 4.9) in the northeastern part of the Mila province, which triggered significant landslides in the El Kherba district and Grarem Gouga city, leading to substantial economic losses. To underpin our analysis, we conducted rigorous fieldwork over several days to establish a comprehensive database of landslides that were induced by the earthquake. The fieldwork also involved scrutinizing the initial slope instability map created immediately after the seismic event. For our analysis, we selected input parameters, such as lithology, slope angle, normalized difference vegetation index (NDVI), distance from rivers and roads, precipitation, and seismic hazard, which is quantified with peak ground acceleration (PGA). This hazard differs from the intensity measured on the MM, EMS, or MSK-64 scales. The seismic hazard, along with all other parameters, is integrated into a GIS environment. Our primary objective is to empirically assess the performance of different fuzzy logic operators in generating landslide susceptibility maps and to evaluate the accuracy of the optimal maps through the use of frequency curves.

REGIONAL GEOLOGIC SETTING

The Neogene basin of Mila is administratively located between Mila and Constantine cities (Fig. 1). It covers an area of about 1091 km^2, with an average altitude of 543 m, the temperature ranges from 0 to 40 °C, fairly heavy precipitation (more than 500 mm/yr), well-developed hydrographic network, and a little plant cover, mainly limited to cereal crops and wild grasses. This low vegetation cover considerably favors soil erosion. The Mila region is also characterized by a rugged topography and is located at the border between two geologic provinces; it seems to have lower seismic hazard than neighboring regions, such as the Constantine or Babors (west side of Mila) area.

The Neogene basin of Mila is part of the large postnappe Constantine basin; it constitutes its western extension. It corresponds to a depression located between the Tellian massifs and the high plains of Constantine. In the north, the reliefs of Msid Aïcha and Mt. Sidi Driss in the east and the Zouahra chain in the west separate the basin from the coastal massifs. The Neogene basin of Mila is bounded in the south by the massif of Ahmed Rachedi and Mt. Akehal, in the west by the Zeghaïa Mountains, and in the east by Mt. Kheneg. All these massifs represent the substratum of the Mila basin, belonging to different paleogeographic domains close together or superposed during the ante-Neogene tectonic phases.

In addition, the Neogene basin of Mila, which serves as the study area, is almost entirely covered by Mio-Pliocene continental deposits, as indicated in Fig. 2.

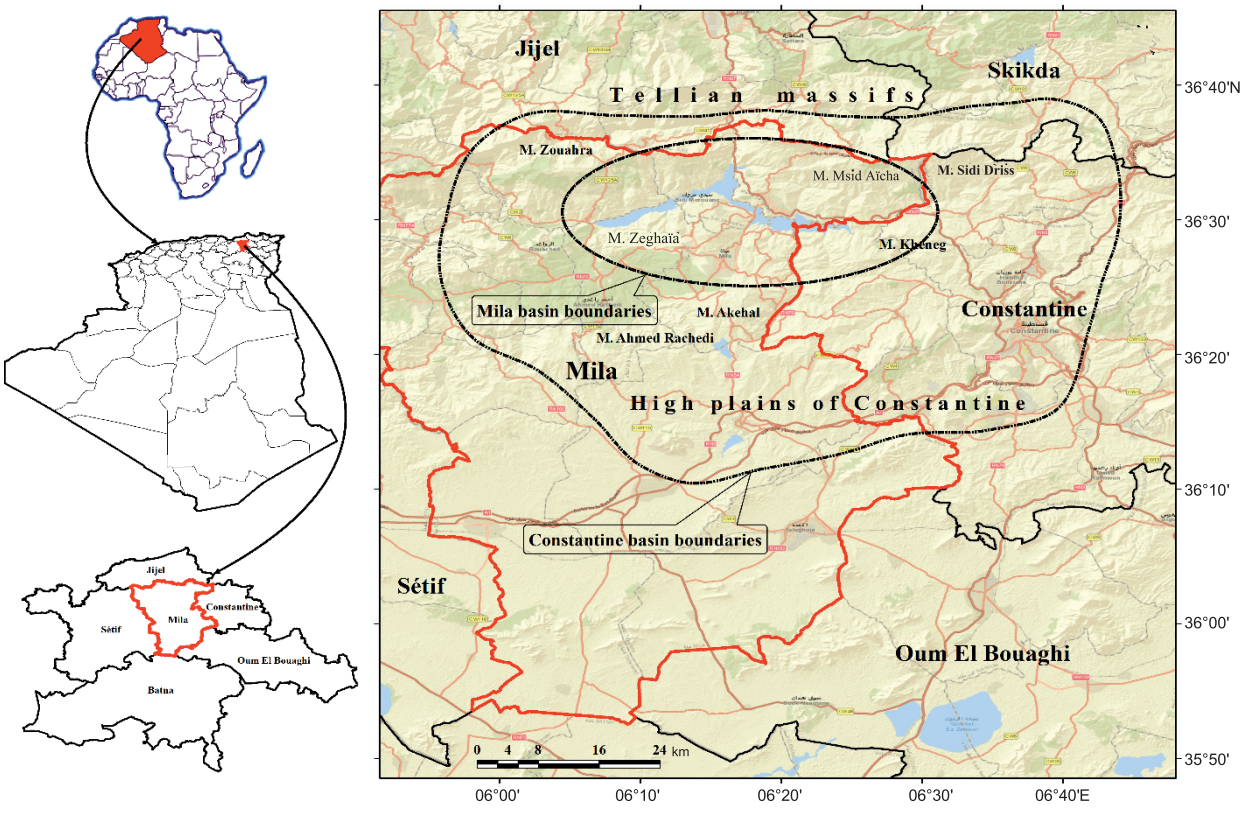

Fig. 1. Location map of the study area.

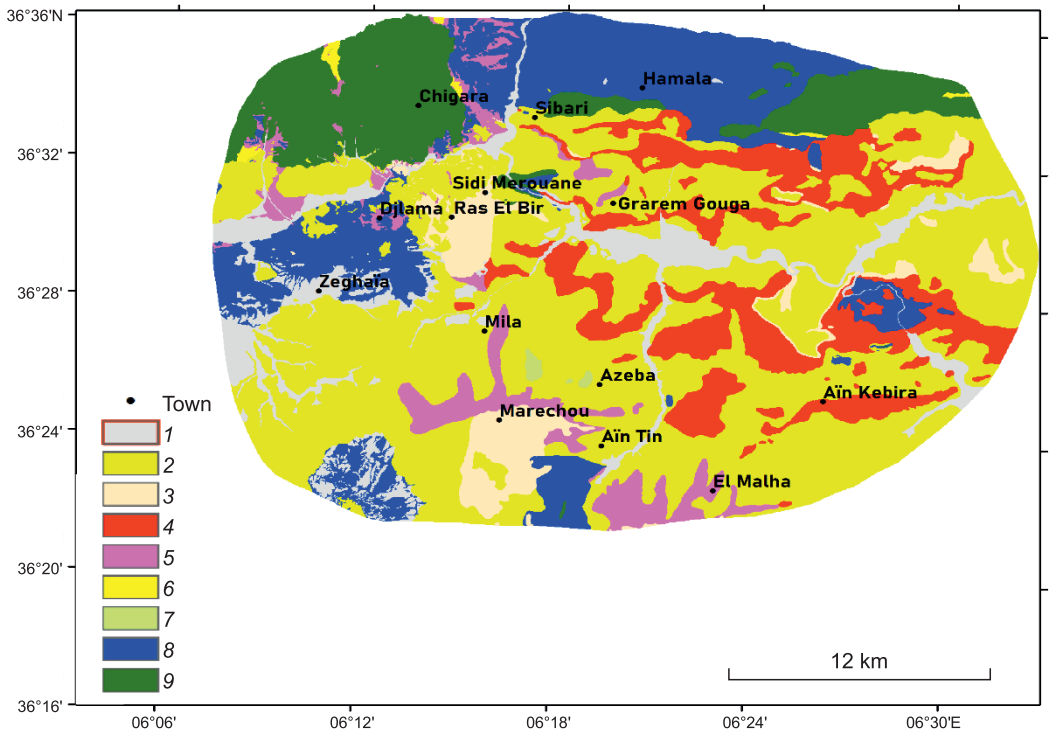

Fig. 2. Lithological scheme of the study area.

1 – Quaternary alluvium and scree; *2* – Miocene sandy clays; *3* – Miocene lacustrine limestone; *4* – Miocene conglomerate and sandstones; *5* – Pliocene limestone scree; *6* – Cretaceous flysch with calcareous microbreccia; *7* – Miocene marine marl; *8* – Cretaceous limestone and marl; *9* – Cretaceous marl and Oligocene sandstone.

Vila (1980) and Coiffait (1992) admit the following succession of Neogene deposits in the Mila basin: (a) gray gypsiferous sandy marls with marine fauna of *Ostrea crassissima*, known as Mila marls (commonly called clays); (b) a basic conglomerate, more or less reddish, with frequent streaks of sandy clays and sandstone lenses at the top; it is highly developed along the Mila Ouadi, known as the conglomerates of Mila Ouadi; (c) irregular alternations of red sandy detrital clays interspersed with some sandstone pastes and conglomerate lenses; (d) some travertine lake limestones exist at the top of this unit (limestone of Sidi Merouane); (e) gray to black marly clays, often with gypsum in their upper part, showing some sandstone levels; and (f) lacustrine limestone, sometimes travertine, white, pink or red, from the Pliocene.

The Quaternary deposits in the Mila basin are represented by actual and recent alluvium of wadis (Oued Rhumel, Oued Endja, and Oued el Kotone), as well as ancient alluvium from terraces, scree, and lacustrine calcareous formations, including limestone crusts. It is essential to note that the predominant deposits covering a substantial surface area in the Mila basin consist of clays and marl altered from Neogene, which are very sensitive to the presence of water, have high plasticity, low shear strength, and low cohesion, and, therefore, constitute zones prone to landsliding.

SEISMOTECTONIC SETTING

The Neogene Mila basin is a part of the Northeast Algeria region, which is located at a convergent boundary of the African and Eurasian tectonic plates. This region is considered an active seismic zone within Algeria (Fig. 3), which has been shaken by several low- to moderate-sized earthquakes during the last few centuries (Ayadi and Bezzeghoud, 2015; Mouloud et al., 2023).

In the selection of seismic catalogs for this research, a thoughtful and comprehensive approach was undertaken to ensure the reliability and inclusivity of the seismic data. Recognizing the global nature of seismic events, we incorporated data from renowned international catalogs, including USGS/NEIC, IGN, and ISC 2014. These catalogs are esteemed for their extensive coverage and meticulous recording of seismic activities on a global scale. To complement this global perspective with localized insights, information from national catalogs was also integrated, drawing upon datasets from the Center of Research in Astronomy, Astrophysics, and Geophysics, Algiers, Algeria (CRAAG)—CRAAG 2002—and the National Center for Applied Research in Earthquake Engineering (CGS)—CGS 2003. This dual-sourced strategy allows capturing both the broader seismic context and the nuances of seismicity specific to the study area.

In the compiled catalog, seismic magnitude data are standardized to moment magnitude (M_w), emphasizing that the relationship between M_s (surface wave magnitude) and M_w in seismotectonics is not a straightfor-

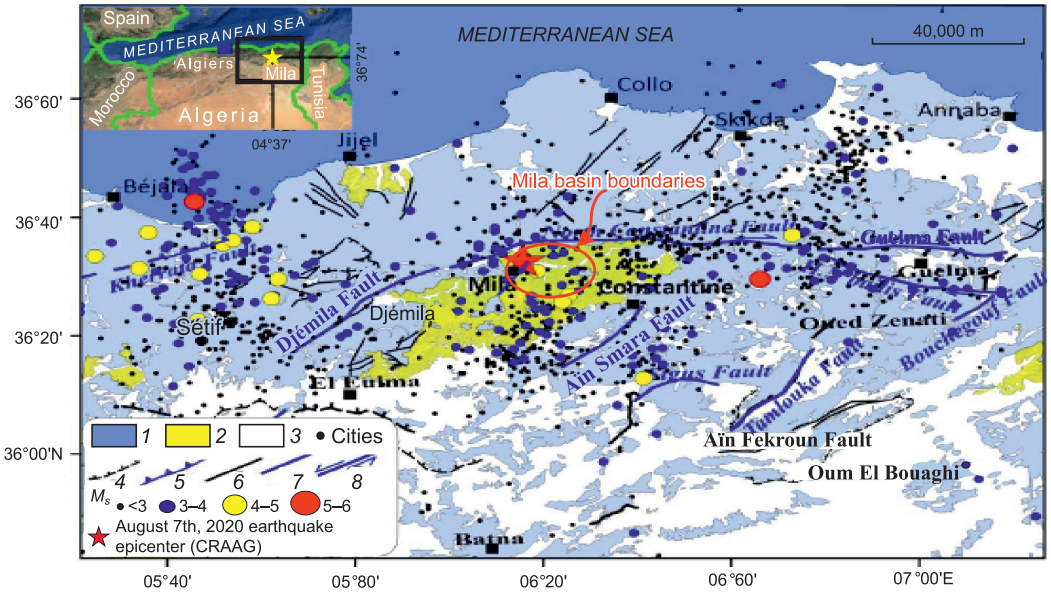

Fig. 3. Seismicity of eastern Algeria. Faults are from (Vila, 1980; Bounif et al., 1987; Meghraoui, 1988; Bouhadad et al., 2003; Kherroubi et al., 2009). The seismicity data are from (Harbi et al., 2007; Ayadi and Bezzeghoud, 2015; Abbes et al., 2019).

1 – sandstone and limestone (Oligocene); *2* – clays, marls, and lacustrine limestones (Mio-Pliocene); *3* – scree and Quaternary alluvium; *4* – hidden faults; *5* – thrust faults; *6* – faults; *7* – active faults; *8* – strike-slip (Vila, 1980; Bounif et al., 1987; Meghraoui, 1988). The red star indicates the epicenter of the Mila earthquake on August 7, 2020.

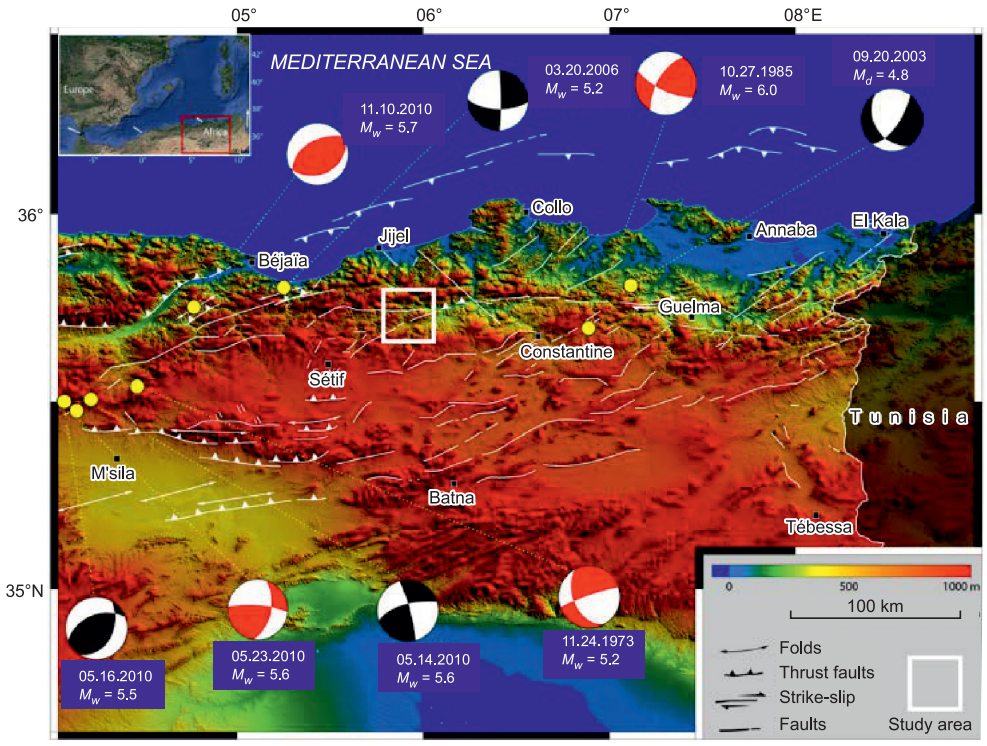

Fig. 4. Seismotectonic framework of eastern Algeria (Meghraoui, 1988; Belabbès, 2009). Focal mechanisms are centroid moment tensor solutions. The focal mechanisms are given after (Bounif et al., 1987; Bouhadad et al., 2009; Ayadi and Bezzeghoud, 2015; Beldjoudi et al., 2016). The white square indicates the localization of the Mila region.

ward, fixed formula. The conversion between these scales varies based on factors like seismic source and depth, often involving empirical relationships like $M_w = a \times M_s + b$, with coefficients determined through regression analysis. The values of specific coefficients may vary by dataset and region if we acknowledge that such relationships are approximations influenced by various factors. This standardization aligns with empirical formulas outlined, for example, in the work by Lolli et al. (2014), addressing the conversion between teleseismic magnitudes and moment magnitude. In addition, the unification process aligns with established methodologies presented in works by Nosov and Bolshakova (2020).

The existing earthquake records reveal numerous instances of seismic activity with comparable magnitudes in this region. As indicated in Fig. 4, the October 27, 1985 Constantine earthquake with $M_w = 6.0$ was the largest instrumentally recorded earthquake in the region (Ousadou et al., 2013). Several other moderate-sized earthquakes were studied, such as the 1856 Jijelli earthquake, which caused a tsunami (Harbi et al., 2007), the 1946 Berhoum and the 1937 Guelma moderate-sized earthquakes (Benouar, 1994), the November 10, 2000 (M_w = 5.7) Beni Ourtilane earthquake (Bouhadad et al., 2003), the Beni Ilmane earthquake sequence (M_w = 5.6) of May 14, 2010 (Beldjoudi et al., 2016), the Laalam earthquake of March 20, 2006, M_w = 5.2 (Abbes et al., 2019), and recently the M_w = 4.9 Mila earthquake (Benfedda et al., 2020).

According to Serkhane et al. (2022) and as shown by the focal mechanism solutions in Fig. 4, the study region is located within the Maghrebides chain. It develops at the foot of the southern limit of the internal zones, such as the internal flysch and the base of the Kabyle Ridge. This area is characterized by a complex neotectonic system including reverse faulting, right-lateral and left-lateral strike-slip owing to NE–SW- to E–W-trending faults, and even normal faulting in the Guelma basin. The several active and/or Quaternary faults surrounding the study area are well described by many authors (Vila, 1980; Meghraoui, 1988; Bouhadad et al., 2003; Harbi et al., 2007; Abbes et al., 2019).

EARTHQUAKE INTENSITY AND DAMAGE LEVEL

The Mila basin experienced a seismic event during the period of July–August 2020. The important events are the July 17, 2020 (M_w = 4.6) event at 08:12 (UTC), the August 7, 2020 (M_w = 4.9) main shock at 06:16 (UTC), and the August 7, 2020 aftershock at 11:13 (UTC) (M_w = 4.4), as well as several other felt aftershocks,

particularly, following the August 7, 2020 (M_w = 4.9) event (Benfedda et al., 2020). These seismic events were recorded by several national seismological stations belonging to the CRAAG.

To assess the damage level, a rigorous field-based investigation was conducted during several days in the Mila basin to prepare a database of triggered landslides in the earthquake-stricken area. The preliminary investigation results show that although the August 7, 2020 (M_w = 4.9) earthquake had a relatively low magnitude, it triggered extensive landslides in the epicentral area, which caused huge damage, including collapse of several constructions and severe damage to dozens of others, making hundreds of people homeless in the El Kherba district (Supplementary Materials, Fig. S1). At the same time, the July–August seismic events induced several landslides that caused damage in all the region of the Mila basin and are not considered by previous studies (Fig. 8; Suppl. Mat., Fig. S2).

CAUSATIVE FAULTS

The study area is cut by numerous faults, normal or reverse, strike-slip and affected by folds spilled, generally, toward the south (Fig. 5). The last earthquakes occurred along the fault zone extending from Guelma in the east to Mila in the west, corresponding to the boundary between pre-Neogene and Neogene domains of Petite Kabylie (Vila, 1980; Meghraoui, 1988; Bendjama et al., 2021). This zone exhibits a series of NE–SW- to E–W-trending fault segments and is characterized by seismicity pattern (Harbi et al., 2007). The eastern segment, known as the Guelma fault, is considered a major right-lateral fault.

In the southeast of the study area, there is the Aïn Smara fault, recognized as active during the Constantine earthquake of October 1985 (Bounif et al., 1987). This fault consists of four segments, spanning nearly 30 km. It is aligned in the NE–SW direction, with a stalling character attested by the focal mechanism of the Constantine earthquake of October 27, 1985 (Bounif et al., 1987). One more, the Sigus fault, oriented E–W and 30 km long, however, is not considered causative (Vila, 1977, 1980). However, this selection of causative faults requires further seismotectonic investigations, including field detailed geological work and seismological/GPS monitoring to clearly identify them.

Regarding the earthquake size distribution, the background historical earthquake intensity (Fig. 6*a*) shows that the largest ancient earthquake in the study area occurred in 1960. This figure shows also the Gutenberg–Richter laws (Fig. 6*b*, *c*). As shown in the earthquake spatial distribution in Fig. 7, no large-magnitude earthquake has been reported in the study area during approximately 260 years for which documented records exist (Ayadi and Bezzeghoud, 2015).

Relating to the focal depth of the latest earthquake (August 2020), a preliminary location analysis of the strong ground motion data suggests a focal depth of 10–12 km (Benfedda et al., 2020). This earthquake is considered to have a shallow depth, according to field observations and macroseismic data analysis.

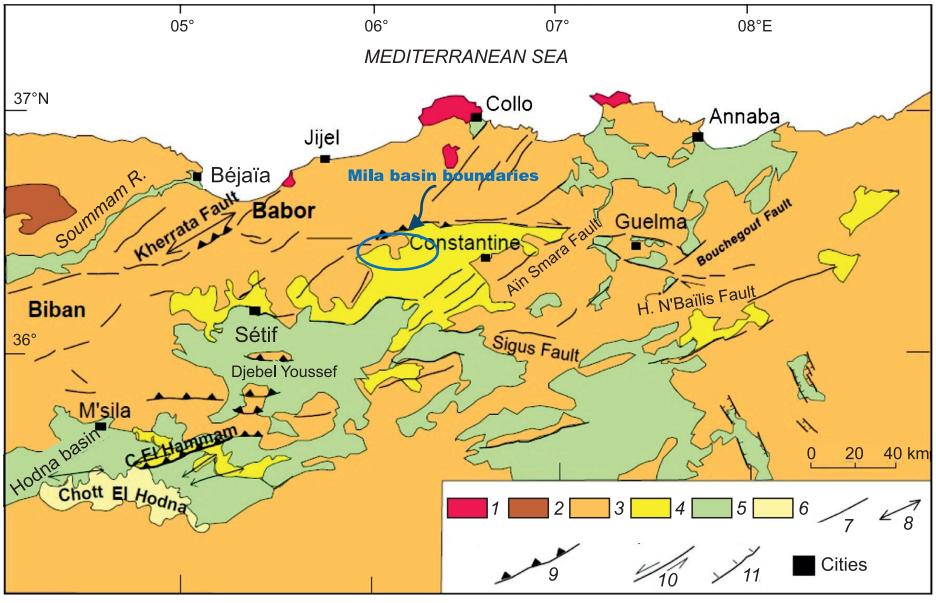

Fig. 5. Causative faults in the study area, from (Meghraoui, 1988).

1 – Tertiary igneous rocks; *2* – Paleozoic shale; *3* – limestone and marl of the Jurassic–Cretaceous and lower Cenozoic basement; *4* – clay and conglomerate of Neogene postnappe time; *5* – Plio-Quaternary lacustrine limestone crust; *6* – Quaternary alluvium; *7* – faults; *8* – anticline; *9* – reverse fault; *10* – strike-slip fault; *11* – normal fault.

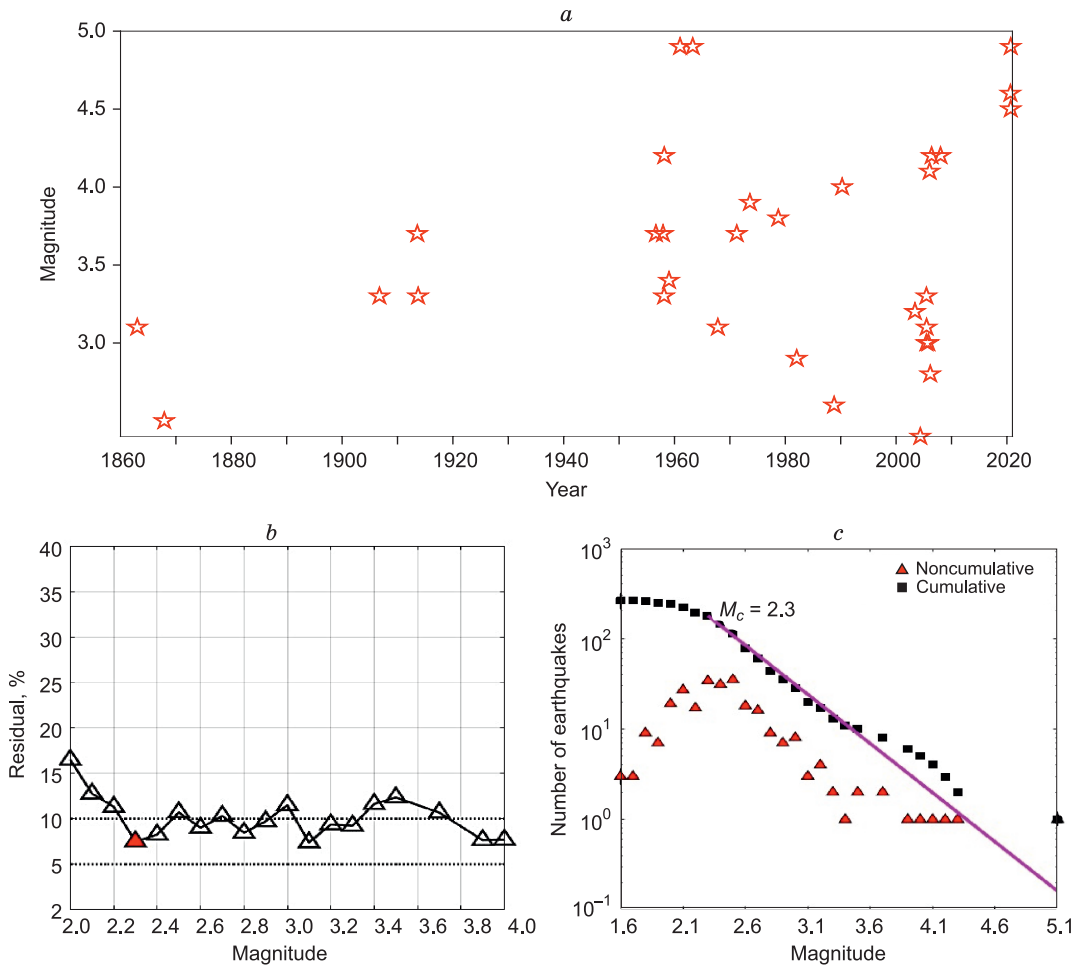

Fig. 6. Earthquake information in the study area.

a – Earthquake historical distribution; *b*, *c* – Gutenberg–Richter laws.

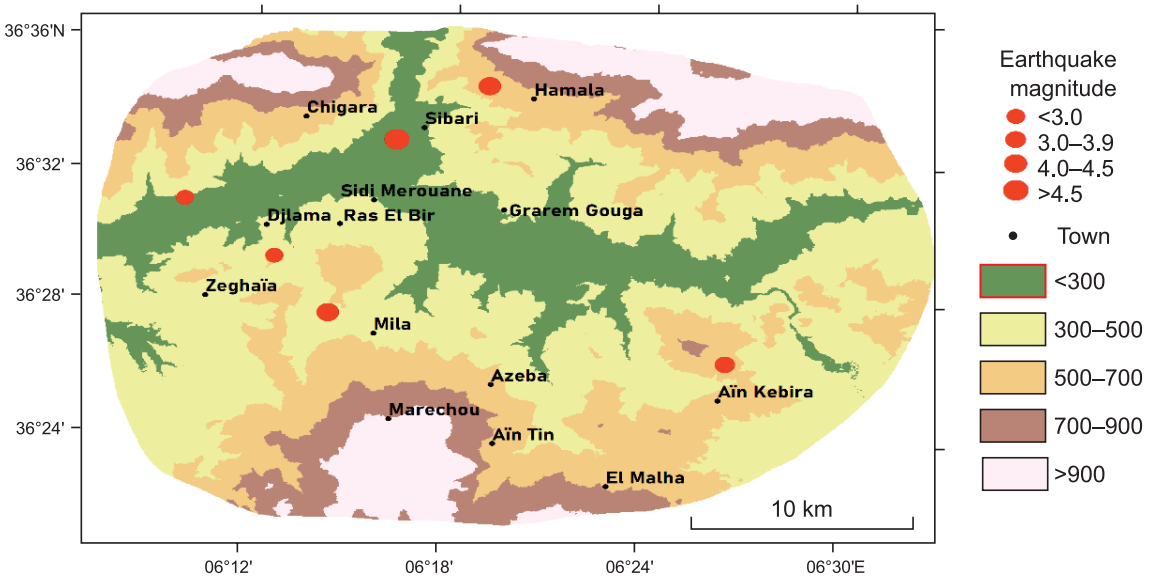

Fig. 7. Earthquake spatial distribution in the study area.

THE FUZZY LOGIC APPROACH

The fuzzy logic is a heuristic approach that was introduced by Lotfi Zadeh (1965) to analyze mathematically nondiscrete natural processes. This approach enables more sophisticated decision-tree processing and better rules-based programming integration. This is kind of generalization of the conventional logic, according to which all claims will not have truth values of zero or one but a partial truth value between zero and one.

If X is a space of objects and x represents one of its generic elements, then $X = \{x\}$. The fuzzy set A in X is characterized by a membership function $\mu_A(x)$, which associates a real number in the interval [0, 1] with each object in X; the value of $\mu_A(x)$ is defined as "the grade of membership" of x in A (Zadeh et al., 1996; Kayastha et al., 2013).

In the case of landslide susceptibility mapping, the spatial objects on a map are considered members of a set, and the expected occurrence of landslides can be also expressed as a fuzzy membership using subjective assessment or/and objective analysis based on fuzzy logic (Lee, 2007). This approach is very interesting in such a case of spatial analysis, because it is easy to use and understand and can be applied to any spatial data from any measuring scale. The desired parameters are measured at discrete intervals in a GIS environment, and the membership function is represented as a table that links map classes to membership values (Tangestani, 2004). For this reason, the fuzzy logic approach makes it possible to combine the weighted maps in more flexible ways and is easily implementable using a GIS modeling language (Razifard et al., 2019). The spatial (e.g., distance from faults) and zonal (e.g., lithology class) entities on a map are considered members of a set when applying fuzzy logic in landslide susceptibility mapping. When two or more maps with fuzzy membership functions for the same set are available, a variety of operators are used to merge the membership values.

In this context, six operators are often utilized in fuzzy logic-based landslide studies: fuzzy intersection (AND), union (OR), complement (NOT), fuzzy algebraic product, fuzzy algebraic sum, and fuzzy gamma. The logical operations AND, OR, and NOT are introduced by Zadeh as extensions of their Boolean origins. These operators are max, min, and $(1 - \mu)$, and they are expressed by equations 1–3:

Union of fuzzy sets:

$$\mu_{combination} = max\left(\mu_A, \mu_B, \mu_C, \ldots\right); \tag{1}$$

Intersection of fuzzy sets:

$$\mu_{combination} = min\left(\mu_A, \mu_B, \mu_C, \ldots\right); \tag{2}$$

Complement of fuzzy set $\backslash A$:

$$\mu_{\backslash A} = 1 - \mu_A \ . \tag{3}$$

The fuzzy operator OR employs the maximum function and is equivalent to the union defined by Eq. 1. In this equation μ_A, μ_B, and μ_C represent the fuzzy membership values of existing pixels in specific situations on different factor maps. In the case of the fuzzy operator intersection, or AND operator, it employs the smallest function for overlaying. This operation is usually used for the dependent parameters as well as evidence required to validate the hypothesis. The complement of fuzzy set A is defined by Eq. 3; however, this operator is not used for overlaying different factor maps.

In addition, the max, min, and complement operators do not reflect the level of compensation by which humans aggregate criteria. Some other fuzzy logic operators are available, and they more accurately represent the human decision-making. Zimmermann (1996) proposed and empirically tested an operator called "gamma operator" (γ), which is more general than the compensation between intersection and union of the fuzzy sets. This operator is defined in terms of the fuzzy algebraic product (Eq. 4) and the fuzzy algebraic sum (Eq. 5) as expressed in equation 6:

The fuzzy algebraic product:

$$\mu_{PRODUCT} = \prod_{i=1}^{n} \mu_i ; \tag{4}$$

The fuzzy algebraic sum:

$$\mu_{SUM} = 1 - \prod_{i=1}^{n} (1 - \mu_i) ; \tag{5}$$

The fuzzy gamma operation:

$$\mu_{combination} = \left(\mu_{SUM}\right)^{\gamma} \times \left(\mu_{PRODUCT}\right)^{1-\gamma} , \tag{6}$$

where μ_i is the membership value of the i factor in the map and γ is a user input in the range [0, 1].

In the case of the fuzzy algebraic product (Eq. 4), the fuzzy membership values in the output map are more likely to be reduced when we use this function. Thus, the combination of elements will have decreasing

effects. In the case of the fuzzy algebraic sum (Eq. 5), when we use this operator, the fuzzified values in the output map are more likely to be increased. As a result, the combination of elements will have an increasing impact, resulting in the maximum risk due to the increasing effects of fuzzy mathematical addition. When the fuzzy gamma operation is used (Eq. 6), if γ is 0, the operator is equivalent to the fuzzy algebraic product, and when γ is 1, it is equivalent to the fuzzy algebraic sum. Selecting correctly γ between 0 and 1 yields flexible output values of all decreasing and increasing tendencies of fuzzy multiplication and addition, respectively.

The fuzzy logic approach was implemented using the Fuzzy Overlay tools within the ArcGIS software. These tools are instrumental in combining multiple criteria by assessing the likelihood of each cell being a member of various sets defined by the criteria. For example, they determine the likelihood that a specific location belongs to the favorable suitability for slope, aspect, and distance to roads simultaneously. The implementation process involves two main steps in fuzzy logic for overlay analysis: fuzzification (fuzzy membership process) and fuzzy overlay analysis. These steps align with the reclassify/transform and add/combine steps, respectively, in the general overlay process. The use of Fuzzy Overlay tools ensures a robust and efficient integration of fuzzy logic into the GIS package.

LANDSLIDE SUSCEPTIBILITY MAPPING METHOD

The landslide susceptibility mapping consists in exploring several causative factors that are effective in increasing landslide susceptibility. In general, there is a close link between geography, geologic history, tectonics, lithology, and geomorphologic evolution of slopes as well as the landslide susceptibility (Li and Wang, 2019). These parameters, when combined, tend to promote or inhibit the slope collapses (Chandrasekaran et al., 2019). In the case of seismically induced landslides, they are frequently caused in the area near active faults or in the epicentral area of earthquakes. As a result, hazard evaluations would benefit from the mapping and study of such a case of landslide distribution.

In this case study, most of the parameters used in the literature are selected. These parameters are "slope," "slope exposure," "lithology," "precipitation," "proximity to faults," "curvatures," "altitude," "proximity to hydrographic networks," "road network," "NDVI," "annual solar radiation," and "earthquake shock intensity." Next, a GIS–fuzzy logic model was used in this study to assess landslide risk in the area affected by the earthquake.

Several fuzzy classes or functions are used to define the transformation or to remap input values to new values based on a function to determine the fuzzy membership for each input value. There are several fuzzy functions: Gaussian, large, small, linear, near, mean and standard deviation (MS) small, and MS large. For example, the large function is useful when the large input values have a higher membership, and the small function is useful when the small input values have a higher membership. In the case of the linear function, it is useful when the smaller values linearly increase in membership to the larger values for a positive slope and opposite for a negative slope. The fuzzification function should be chosen based on the criteria importance, nature, and relationship with the target. As the fuzzy logic model was used to map landslide susceptibility using raster analysis, each pixel should be assigned a membership value ranging from 0 to 1 in relation to the ideal function. Table 1 shows the fuzzy membership function types that were used for fuzzification in each factor for all the measured parameters.

The performance of various fuzzy operators in landslide susceptibility mapping was used by applying fuzzy operators: intersection (AND), union (OR), algebraic sum (SUM), multiplication (PRODUCT), and different fuzzy gamma values of fuzzy overlay—to determine the membership function of each criterion and superposed information layer to detect zones susceptible to a landslide in the study area. The landslide susceptibility zonation maps were categorized: "very high, high, moderate, low, and very low." The results were validated by the computing area under the receiver operating characteristic (ROC) curve. The ROC statistical validation allowed identifying the most efficient method. Finally, the risk map was obtained by the combination of the susceptibility to landslides and the vulnerability map.

As previously stated, the information used in this study was derived from Landsat and Aster satellite photos, the digital elevation model (DEM) obtained from the NASA Shuttle Radar Topography Mission Global (SRTMGL1), the 1: 50,000 geology maps provided by the Algerian Geological Surveys Agency (ASGA), and several other maps provided by County Mila.

Table 1. **The different function types of fuzzy membership of landslide parameters**

Parameter	Slope	Exposure	Lithology	Rain	Fault	Curvature	Altitude	River	Road	NDVI	Solar	Shock
Function type	Linear	Small	Large	Large	Small	Large	Large	Small	Small	Large	Large	Large

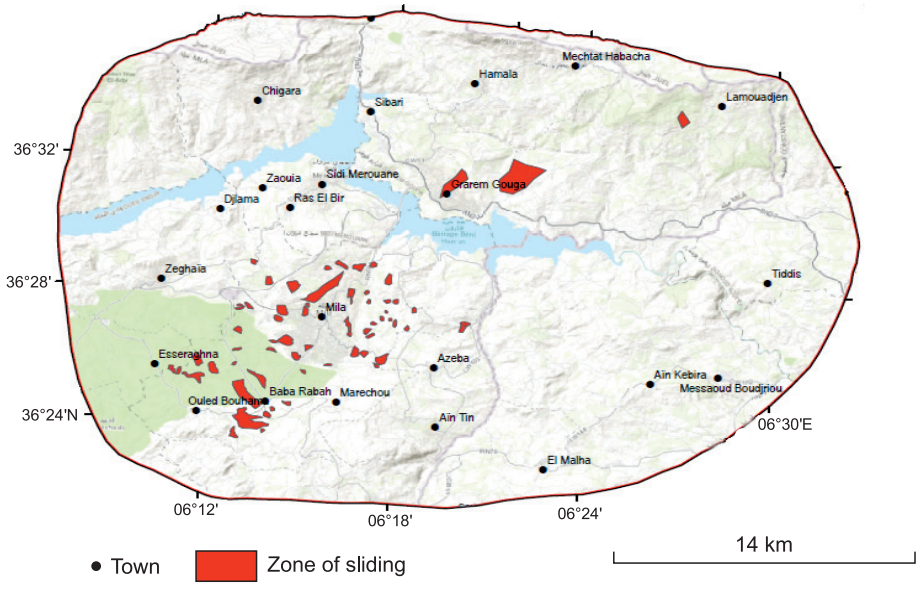

Fig. 8. The earthquake-induced landslides inventory map of the study area.

EARTHQUAKE-INDUCED LANDSLIDES INVENTORY MAP

The landslide inventory map serves as the basis for landslide susceptibility mapping and aids in understanding the variables and circumstances influencing landslides. This is the most important and initial step, because future landslides are expected to occur in the same geologic, hydrologic, and geomorphic conditions as those in the past. In addition, the current landslides are taken into account to validate the results of such kind of study.

The earthquake-induced landslides inventory map of the study area (Fig. 8) has been made using the diachronic interpretation of Landsat 8 satellite images, topographic data, historical records provided publicly by the local municipality, and exhaustive fieldwork. This map gives information on the spatial distribution of the instabilities in relation with the case study. In general, the mapped landslides are both shallow (depth <5 m) and deep-seated (depth >5 m). They mainly occur in the Neogene complex and the central middle part of the basin and vary from simple localized sliding to large-scale movement.

In addition to this preliminary work, the field investigation of landslides caused by the earthquake indicates that most of them are soil slides. In the epicentral area, a few hours after the main shock, the cracks of the upstream part of the large-scale movement (Fig. 9*a*) started to develop in the El Kherba district and propagate on the ground surface along more than 2 km, resulting in the collapse of several buildings and serious damage

Fig. 9. Nature of landslides induced by earthquake in the El Kherba district.

a – Large movement scale; *b* – soil slide.

in various local utilities. Those movements resulted in a landslide with a total length of 2.2 km, a width of 1.2 km, and an approximate area of 2.64 km^2. In other regions of the study area, far from the epicentral area, the landslides are mainly soil slides, rock slides, and rock falls, depending of the nature of the land, and are all noticed shortly after the earthquake occurs (Fig. 9*b*). Globally, landslides generated by seismic events in the case study have covered an area of over 9.5 km^2.

CAUSATIVE FACTORS RELATED TO LANDSLIDES

The geoenvironmental characteristics of an area control the initiation of slope failures in many ways. They could be considered conditioning factors in the prediction of a phenomenon. In this research, both predisposition and triggering factors were selected (Fig. 10) among those most used in landslide susceptibility assessment.

It is important to note that geomorphometric factors, such as slopes, contours, and aspects, are frequently used in landslide susceptibility analysis, because land types have a significant impact on slope instability, either directly or indirectly, by (1) increasing or decreasing shear strength; (2) controlling microclimatic parameters, such as exposure to sunlight, wind, rainfall intensity, and slope material properties; and (3) controlling landscape forms (Merghadi et al., 2018).

In addition, landslide occurrence is linked to density and proximity parameters (distance to faults, distance to the hydrographic network, and distance to road networks). These parameters cause (1) shear strength and cohesion, (2) permeability, (3) slope material deterioration, (4) slope footing erosion, and (5) saturation (Conforti et al., 2014). Furthermore, a reclassification process was performed for the geometric factors using geometric intervals because of the data distribution uniformity. However, the lithology remains unchanged. A brief description of these factors is given below.

In this case study, the DEM has a resolution of 30 m. It was obtained from the NASA Shuttle Radar Topography Mission Global (SRTMGL1). From these data, several factors were extracted: the slope map (Fig. 11*a*), the elevation or contour map (Fig. 11*b*), and the aspects map (Fig. 11*c*). The slope angle is considered the most important causative factor for landslides because of the action of gravity. In theory, an increase in the slope angle causes an increase in shear stress, which leads to increased slope instability. The slope angle of the present study area was categorized into five classes: (1) <5°, (2) 15–15°, (3) 15–25°, (4) 25–35°, and (5) >35°. The slope angle grouping into five classes at specific intervals is based on the widely employed natural breaks classification method, which optimally divides numerical values to assess landslide susceptibilities. This statistical approach minimizes average deviation within each class and maximizes mean deviation between classes, ensuring an effective categorization of slope parameters obtained through the slope unit method. The elevation map presents the spatial variation of altitude of the study area. This causative factor is important, because higher frequency of landslides is more often observed at higher elevation than at lower elevation; they are common within more or less the same elevation of 1500–1800 m (Bamutaze, 2019). In this study area, the elevation varies from 220 to 950 m. In the case of the slope aspect map, it presents the direction which the slope faces. Landslides are more likely to affect slopes facing rainfalls and the Sun than slopes in edge zones. The slope aspect was categorized into five classes: (1) north (N), (2) east (E), (3) south (S), (4) west (W), and (5) flat.

The rainfall map (Fig. 11*d*) was generated according to the rainfall data from several local meteorological stations using the inverse distance weighted approach. This causative factor is important, because many landslides occur after rainfall exceeding a certain threshold value in terms of rain intensity or duration. Heavy rain or precipitation changes the pressure within the slope, resulting in slope instability. As a result, the heavy water-laden slope materials will yield to gravity forces. The rainfall of the case study was categorized into five classes: (1) <500, (2) 500–550, (3) 550–650, (4) 650–700, and (5) >700. The precipitation classification is determined also by the natural breaks classification method, a statistical approach commonly used for landslide susceptibility assessments. While there might not be a specific regulatory document referenced, the classification aligns with established statistical practices.

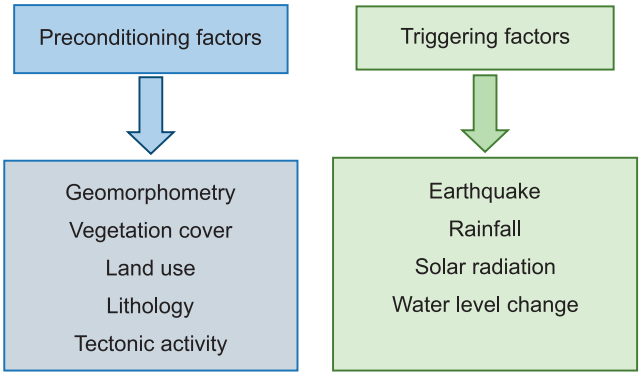

Fig. 10. Selected landslide causative factors.

In the case of annual solar radiation map (Fig. 11*e*), higher annual solar radiation indicates a lower possibility of landslides. The link between solar radiation and landslides is represented by various environmental processes. Solar radiation influences vegetation growth, impacting slope stability by affecting the density and strength of vegetation cover. This factor is crucial to the slope stability. Tree

roots strengthen soil layers, anchor soil to bedrock, and form buttresses to prevent soil movement. Trees also reduce the risk of landslides by lowering soil moisture levels through interception, evaporation, or transpiration. Additionally, solar radiation contributes to evapotranspiration and temperature fluctuations, influencing soil moisture content and the mechanical properties of geologic materials. Understanding the nuanced connections between solar radiation and these factors is essential for assessing landslide susceptibility in different regions.

According to the literature, the normalized difference vegetation index is an effective tool for differentiating and classifying the density of vegetation cover in a region. The NDVI map of the study area (Fig. 11*f*) was

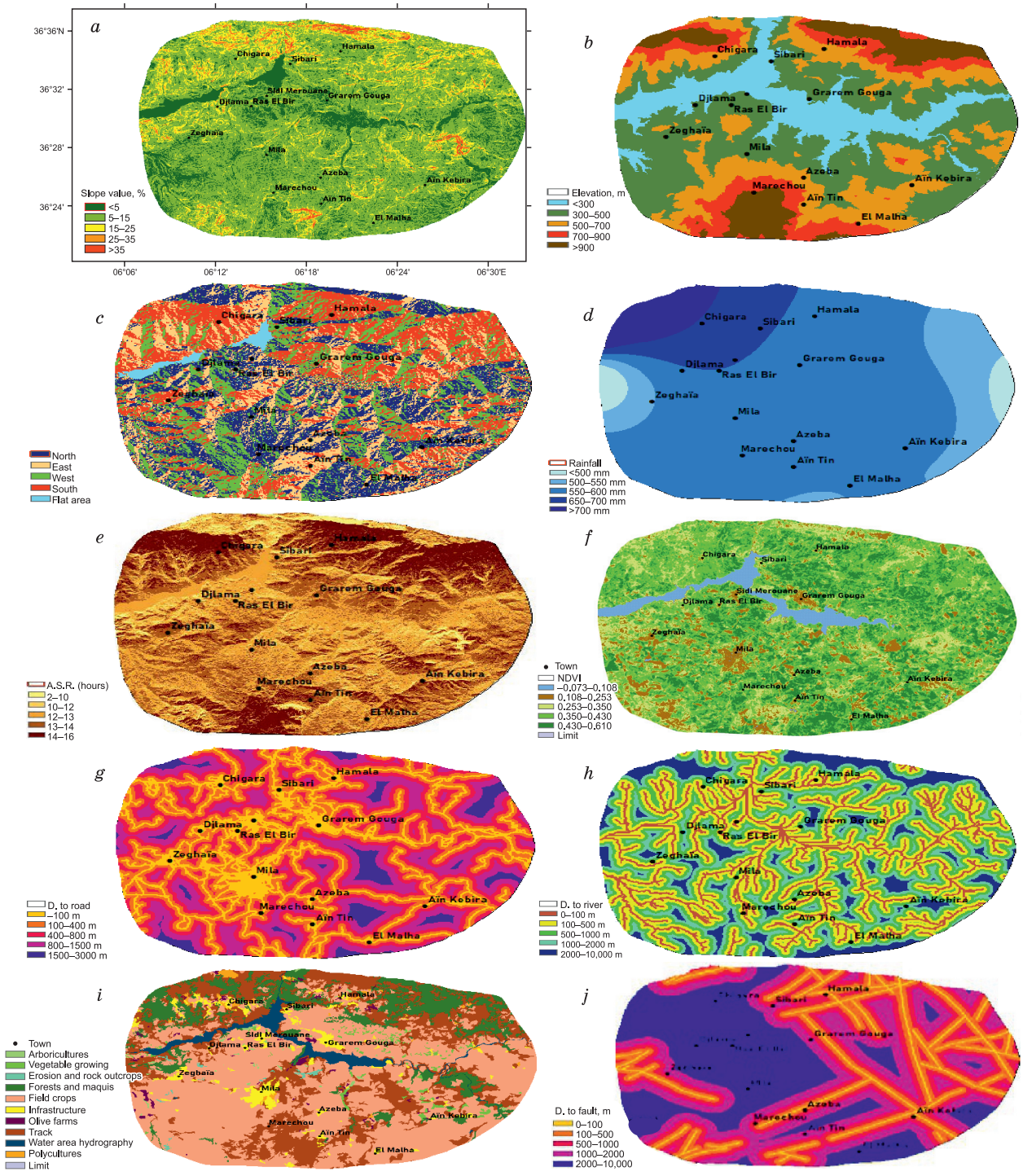

Fig. 11. The selected causative factors related to landslides.

a – Slope; *b* – elevation or contour; *c* – aspects; *d* – rainfall; *e* – annual solar radiation; *f* – NDVI; *g* – distance to river; *h* – distance to roads; *i* – land cover; *j* – distance to fault.

prepared using a GIS software environment by analyzing remote sensing measurements of Landsat 8 data. The resultant values were reclassified into five groups from –0.073 to +0.610.

The distance to river (Fig. 11*g*) was considered to assess the effect of drainage on landslide occurrence. All research in the field has shown that proximity to streams has a significant impact on landslide occurrence, as intensive runoff is frequently the primary cause of mass wasting. The corresponding data for this parameter were extracted from the digital elevation model; this parameter was calculated by the GIS Euclidean distance tool, and the resultant values were reclassified into five groups: (a) <100 m, (b) 100–500 m, (c) 500–1000 m, (d) 1000–2000 m, and (e) >2000 m. It is important to note that almost all the slope instabilities occur in zones less than 100 m from the stream.

Road construction has a significant impact on slope stability. It is a human modification of the old natural existing land through major excavations or vegetation removal that causes sliding. In such a case, the landslide susceptibility increases as we approach the road. The distance to roads map (Fig. 11*h*) was calculated by the GIS Euclidean distance tool, and the resultant values were reclassified into five groups: (a) <100 m, (b) 100–400 m, (c) 400–800 m, (d) 800–1500 m, and (e) >1500 m.

Land use has an impact on the occurrence of landslides. The land cover map of the study area (Fig. 11*i*) was elaborated using a supervised classification in a GIS environment. The study area contains a variety of land uses, including cultivated and built-up areas, forests, grassland, bare land, water bodies, and barren land.

One of the most important factors influencing landslides is lithology (Fig. 7). Each lithologic formation differs in its geotechnical properties and, consequently, in degrees of susceptibility to landslides. This map was generated from the geological maps at a scale of 1 : 50,000 provided by ASGA Company. This factor was well explained in the "Regional geologic setting" section. In addition, the distance to fault was considered (Fig. 11*j*), because landslides are expected to occur near faults and decrease as distance increases. The distance to faults map was calculated using the GIS Euclidean distance tool, and the resultant values were reclassified into five groups: (a) <100 m, (b) 100–500 m, (c) 500–1000 m, (d) 1000–2000 m, and (e) >2000 m.

SEISMIC HAZARD ASSESSMENT OF THE STUDY AREA

The seismic hazard assessment and mapping of the study area were carried out using the CRISIS probabilistic seismic hazard estimation software. This software was developed by Ordaz et al. (2013). The results consist in seismic hazard curves, uniform hazard spectra, and hazard maps showing peak ground acceleration, in several spectral periods and for three levels of ground shaking (50, 10 and 2% probability of exceedance in 50 years). These spectral periods and the different levels of ground shaking are commonly applied in Algerian seismic building codes. For the purpose of estimating ground motion at different points as close as possible, the study area was divided into grids of size 0.1° × 0.1°. In the computational scheme, parameters, such as a, b, M_c, and M_{max}, and attenuation models are the input parameters in the CRISIS program, and peak surface accelerations are the output parameters. The results obtained were prepared in tabular format and used in the CRISIS program to introduce effects of the user attenuation model. The estimated PGA was presented in the form of zone maps for different return periods, such as the calculation at the return period of 475 years (Fig. 12*a*), which corresponds to the probability of exceedance of 10% in 50 years.

In addition, to further enhance the seismic hazard map, Fig. 12*b* represents the earthquake intensity map in the EMS98 scale (from (Mouloud et al., 2023)). It is important to mention that the process of developing a probabilistic seismic hazard map involves identifying seismic sources that impact the area of interest and determining seismicity parameters for each zone. These parameters include seismic activity rate λ, the maximum expected earthquake magnitude M_{max}, and the Gutenberg–Richter b value. The critical step in this process is preparing a homogeneous earthquake catalog through declustering data, involving the removal of aftershocks and foreshocks.

Additionally, the results include peak ground acceleration and spectral acceleration for periods of 0.2 and 1.0 s along with spectral acceleration graphs (Fig. 13*a*, *b*). These comprehensive finds provide a detailed understanding of seismic hazard characteristics in the study area.

LANDSLIDE SUSCEPTIBILITY MAPPING USING FUZZY LOGIC

The earthquake-induced landslides susceptibility maps were elaborated by combining several causative factors (geomorphometric factors, rainfall, annual solar radiation, vegetation cover, distance to river, distance to road, land cover, lithology, distance to faults, and seismic hazard intensity map) and using the fuzzy operators AND, OR, the algebraic sum, the algebraic product, and different fuzzy gamma values (0.2, 0.5, 0.8, and 0.9). The results are displayed in Fig. 14.

It is important to clarify that the integration of simple algebraic functions, such as addition and multiplication, in GIS-based analyses is a widely accepted and well-established practice. These operations serve as

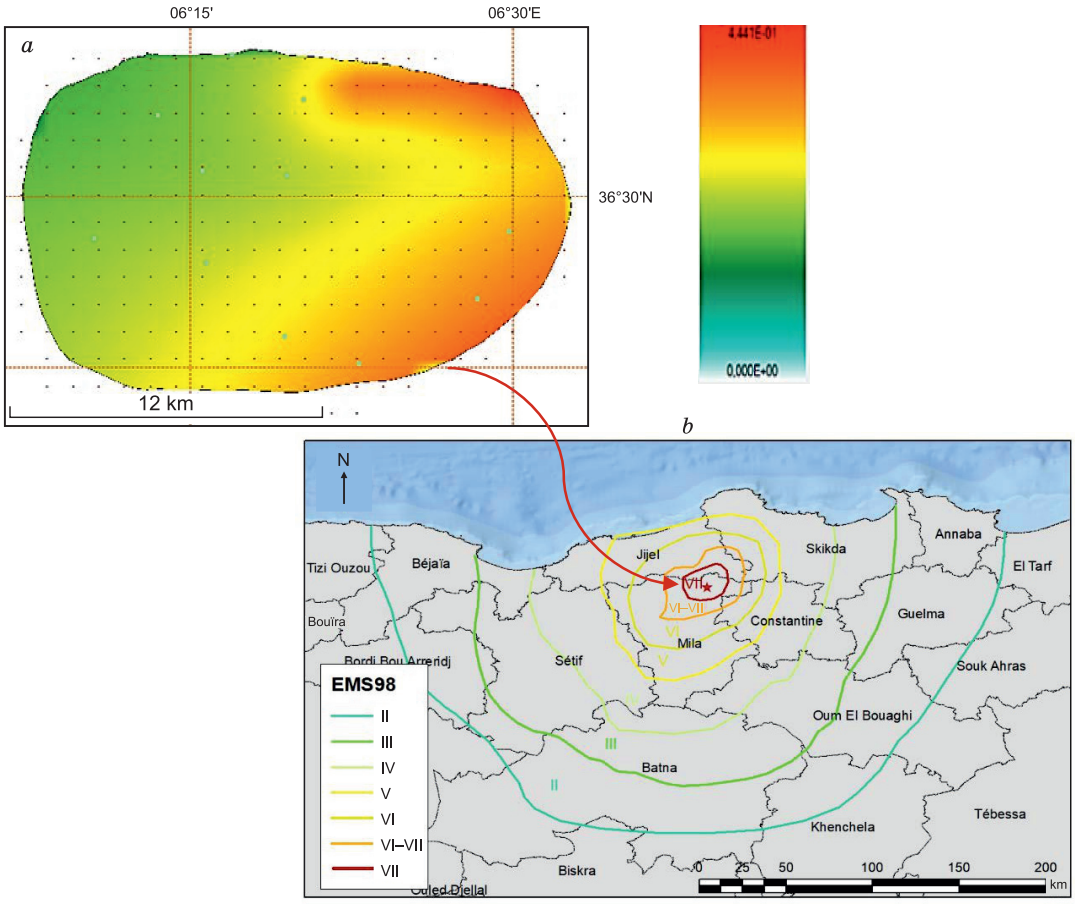

Fig. 12. The seismic hazard scheme of the study area at a return period of 475 years (*a*) and the earthquake intensity map at the EMS98 scale (from (Mouloud et al., 2023) (*b*).

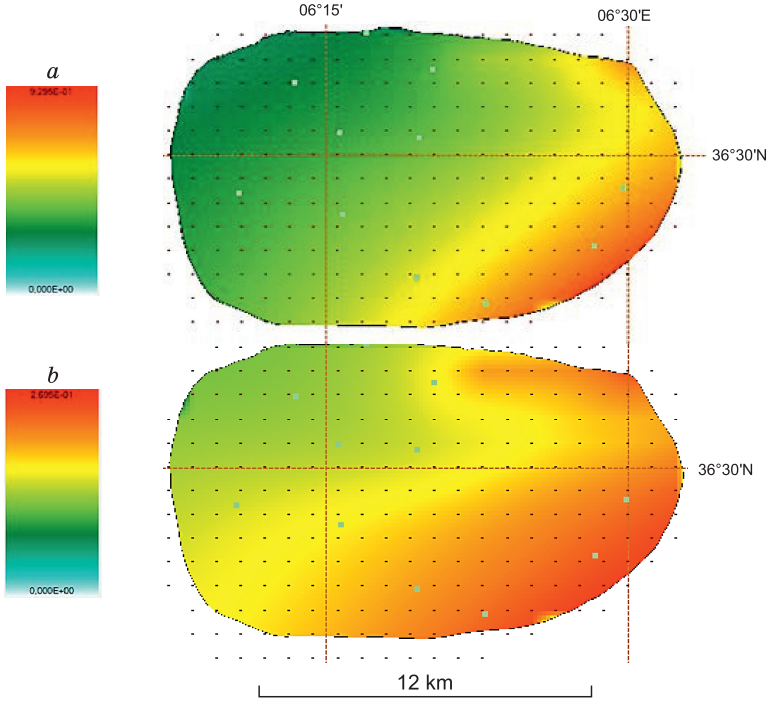

Fig. 13. Seismic hazard schemes of the study area. *a* – For a spectral acceleration of 0.2 s; *b* – for a spectral acceleration of 1.0 s.

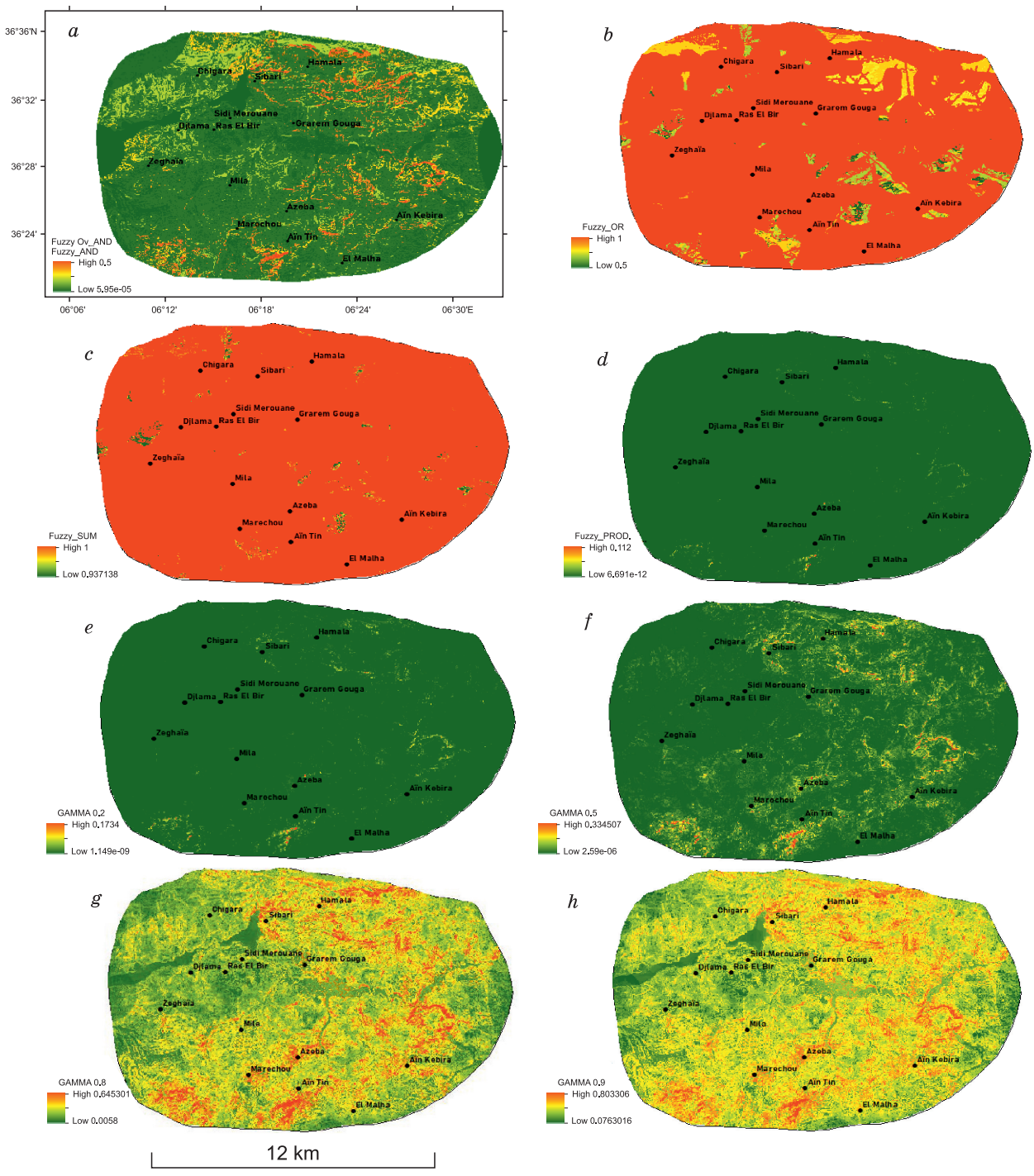

Fig. 14. Landslide susceptibility schemes created using fuzzy logic operators.

a – AND; *b* – OR; *c* – sum; *d* – product; *e* – gamma 0.2; *f* – gamma 0.5; *g* – gamma 0.8; *h* – gamma 0.9.

fundamental tools in spatial analysis, enabling the synthesis of diverse geospatial information. In the presented methodology, these operations were utilized to amalgamate various factors contributing to landslide susceptibility, producing comprehensive maps that depict the cumulative impact of each factor. Additionally, the incorporation of fuzzy logic overlay further enhances the realism of the analysis by accommodating the inherent uncertainty and gradual transitions present in spatial data. Together, these techniques contribute to the robustness and accuracy of our GIS-based landslide susceptibility mapping.

Figure 14*a* presents the results of applying the fuzzy operator AND. The map shows that the study area is characterized by moderate susceptibility for almost all the parts, except those near the epicentral zone of the

last earthquake or near the higher slope location, or closer to the fault. This might be because the AND operator extracts the minimum degree of membership by selecting the minimum value (weight) of the information layers of each pixel and considering it in the final map (Razifard et al., 2019). Figure 14*b* shows the results of applying the fuzzy operator OR. The resulting map indicates that the study area is characterized by very high susceptibility to landslides.

This outcome can be elucidated, because the OR operator will display the highest value found in the sets to which the cell location belongs. In other words, it helps to identify the location that has at least one of the criteria being fully in the suitable set. Figure 14*c* shows the earthquake-induced landslide susceptibility maps by applying the algebraic sum. The resulting map by this operator presents very high landslide susceptibility similar to those obtained from the fuzzy OR. This result can be explained, because this operator will add the fuzzy values of each set the cell location belongs to. The resultant sum is an increasing linear combination function based on the number of criteria entered into the analysis. In the reverse case, when we use the algebraic product (Fig. 14*d*), the resulting map shows that the study area is characterized by moderate landslide susceptibility. This operator will multiply each of the fuzzy values for all the input criteria. The resulting product will be less than any of the input, and the value can be very small. Figure 14*e*–*h* presents the earthquake-induced landslide susceptibility maps by applying different fuzzy gamma values (0.2, 0.5, 0.8, and 0.9). This operator is the algebraic product of the fuzzy product and fuzzy sum raised to the power of gamma. If gamma is set to 1, the output is the same as the fuzzy sum; if gamma is set to 0, the output is the same as the fuzzy product. This operator compromises the increasing effect of the fuzzy sum and the decreasing effect of the fuzzy product, because the values in the middle allow combining the product between these two extremes and may be different from fuzzy AND or fuzzy OR.

VALIDATION OF THE MODELIZATION

The validation process is critical in such studies, because it is necessary to assess the model accuracy by comparing the result with the real landslide regions. According to literature, there are numerous methods; however, the receiver operating characteristic (ROC) analysis method is widely used for assessing predicting models in GIS-based studies. The ROC curve is elaborated by plotting the true positive rate against the false positive rate at several threshold settings, and the indicator frequently used to evaluate the model performance is the area under the curve (AUC). This AUC score varies between 0 and 1. A perfect predictor has an AUC score of 1.0, while a random guess predictor has an AUC score of 0.5. The AUC results were judged outstanding for AUC values ranging from 0.9 to 1.0, excellent for AUC values ranging from 0.8 to 0.9, acceptable for AUC values ranging from 0.7 to 0.8, and poor for AUC values ranging from 0.5 to 0.7 (Swets, 1988).

The area under the curve for the fuzzy AND operator is 0.818, implying acceptable overall success score accuracy of 81.80% (Suppl. Mat., Table S1). However, as mentioned in Fig. 14*a*, the landslide model shows that most of the study area has very low landslide susceptibility, except some parts with just moderate susceptibility. These results suggest a lower estimation of the landslide strength.

Regarding the fuzzy operator OR, the algebraic sum, and the algebraic product, they give higher AUC score rate, ranging from 94.3 to 97.0%. However, in the case of the OR and SUM operators, as seen in Fig. 14*b*, *c*, their landslide susceptibility values are higher than the expected level for most parts of the study area, suggesting a higher overestimation. Inversely, in the case of the algebraic product operator (Fig. 14*d*), it gives a lower estimation of most of the study area. These outcomes indicate that the resulting maps and their fuzzy operator are not suitable for assessing landslide susceptibility.

In the case of the gamma operators, they seem clearly to produce excellent results, with AUC score accuracy ranging from 82.1 to 96.2%. The fuzzy gamma operator for values equal to 0.1 and 0.2 gives higher AUC score even if the resulting maps show very low susceptibility of most of the study area. It seems that the gamma operator for the value equal to 0.8 generates very evenly spread combined fuzzy membership values, with AUC score accuracy of 83.1%. These results are demonstrated by its achievements in physical prediction of landslide locations, as shown in Supplementary Materials, Fig. S3.

ASSESSMENT AND ANALYSIS OF OBTAINED RESULTS

As a result, the final landslide susceptibility map should be derived from the combined fuzzy membership map obtained with the fuzzy gamma operator for $\gamma = 0.8$. This map is divided into low, moderate, high, and very high landslide susceptible zones (Fig. 15*a*). In addition, to evaluate the effect of adding or removing the seismic hazard as a causative factor, Fig. 15*b* was added, showing an earthquake-induced landslide susceptibility map with the fuzzy gamma operator for $\gamma = 0.8$ but without integrating the seismic hazard. The AUC results in the case of fuzzy gamma operators for $\gamma = 0.8$ with seismic hazard intensity (83.1%) are better than AUC results in

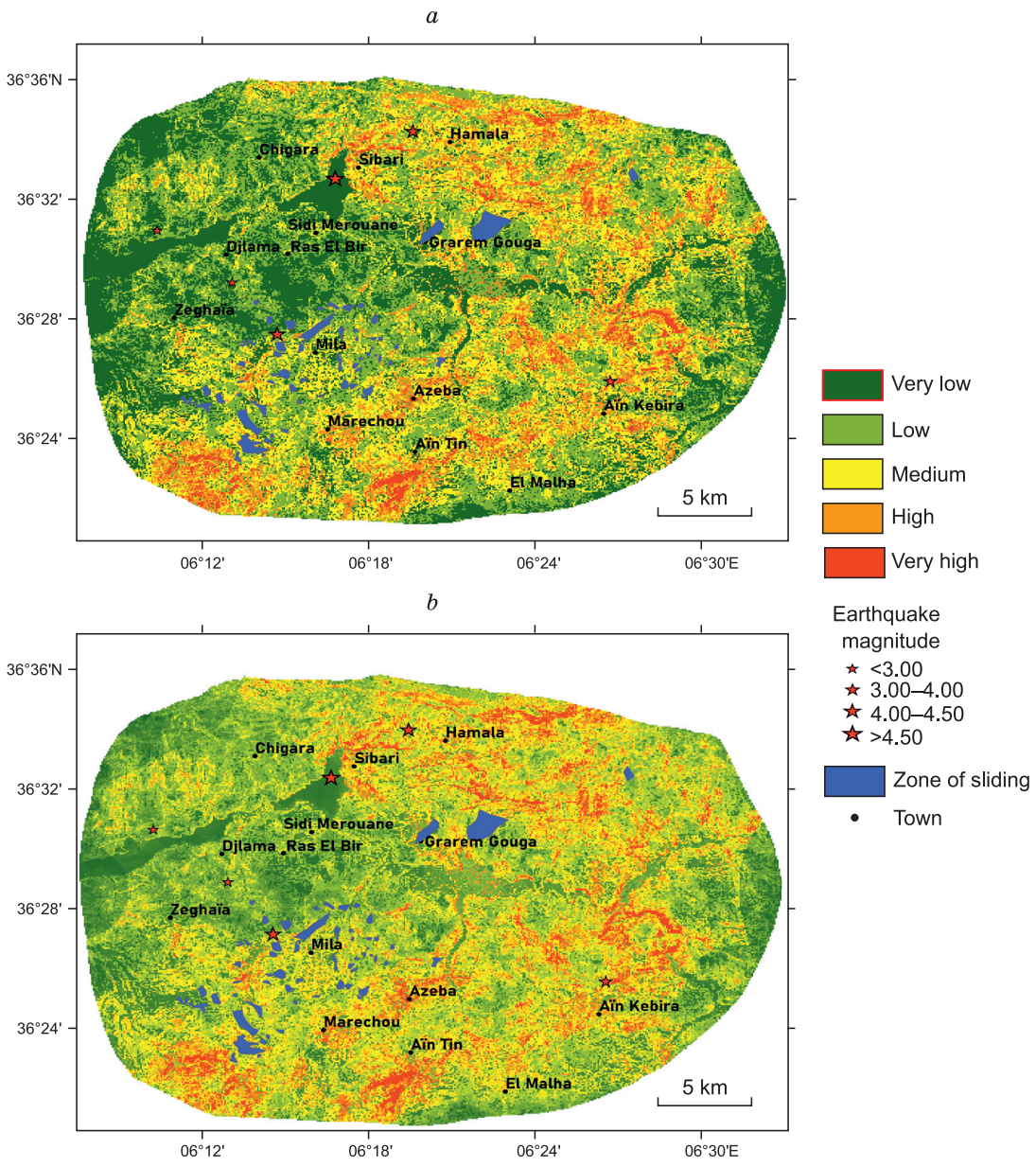

Fig. 15. Landslide susceptibility schemes created using gamma 0.8.

a – With earthquake; *b* – without earthquake.

the case without adding seismic hazard intensity (76.9%). It is evident that including the seismic hazard as a causal element improves the accuracy of locating the landslide that may be induced by an earthquake.

Inspired by the index of neotectonic activity, the presented methodology is distinguished by introducing seismic hazard as a key element, firmly grounded in physical principles. In contrast to the mentioned index, which relies solely on morphometric parameters (Manchar et al., 2022), the limitations of such data operators are acknowledged. Through the incorporation of seismic hazard, supported by a robust physical basis, an enhancement in the precision and reliability of landslide susceptibility assessments is expected. This strategic integration not only enriches the comprehensiveness of the model but also addresses concerns associated with simplistic reliance on morphometric parameters.

To measure physically the accuracy of the obtained results, the landslide susceptibility zones displayed on maps in Fig. 15*a*, *b* can be compared and verified with field information on the earthquake-induced landslide inventory map, particularly for the highly and very highly susceptible zones. Table 2 shows the quantitative comparison with the observed landslide inventory. The results reveal that in the case of including the seismic

Table 2. **Physical validation of landslide susceptibility distribution for the several fuzzy operators**

Susceptible zones	Landslide surface distribution					
	With earthquake			Without earthquake		
	Total (km^2)	Inside inventory area (km^2)	Density (%)	Total (km^2)	Inside inventory area (km^2)	Density (%)
Very low	231.21	9.9413	12.96%	198.30	10.1850	13.26%
Low	276.98	19.6710	25.65%	304.80	23.0810	30.05%
Moderate	238.87	29.6130	38.61%	239.70	26.8700	34.98%
High	104.34	13.7330	17.90%	108.50	13.1340	17.10%
Very high	25.54	3.74150	4.88%	25.46	3.5397	4.61%

hazard map, the very highly, highly, and moderately susceptible zones account for 61.39% of the total observed landslide occurrences, while the surface of these zones accounts for 56.69% in the case of a map without including the seismic hazard map. This trend is the same in the case of zones with low and very low susceptibility, which account for 38.61 and 43.31%, respectively. These results indicate that including the seismic hazard map is better in terms of physical validation**.**

Furthermore, when comparing the AUC scores with and without the inclusion of earthquakes (Fig. 16*a*, *b*), it is evident that incorporating seismic hazard enhances the AUC score, resulting in more accurate modeling compared with the actual occurrence of landslides. These finds strongly suggest that integrating seismic hazard information improves the physical validation of the model.

CONCLUSIONS

This study focused on assessing the susceptibility of landslides triggered by earthquakes in the Mila basin, employing fuzzy logic membership functions and a combination of various contributing factors, including geomorphometric elements, precipitation, annual solar radiation, vegetation coverage, proximity to rivers and roads, land cover, lithology, distance to faults, and a seismic hazard intensity map. An array of fuzzy operators, namely, AND, OR, algebraic sum, algebraic product, and gamma operators with different gamma values (0.2, 0.5, 0.8, and 0.9), was applied to enhance the accuracy of seismically induced landslide mapping. This study pursued two objectives. First, it aimed to derive a seismically induced landslide susceptibility map with the highest attainable precision. Second, it sought to underscore the pivotal impact of integrating the map of seismic hazard as a contributing factor in identifying earthquake-induced landslide-prone areas.

The finds unequivocally indicate that, among the various fuzzy operators examined, the fuzzy gamma operators with a gamma value of 0.8 consistently yielded the most accurate results for earthquake-induced landslide mapping. Moreover, the results emphasize the significance of incorporating the map of seismic intensity as a causative factor in identifying regions susceptible to earthquake-induced landslides. This inclusion serves the dual purpose of safeguarding human lives and minimizing the potential damage to infrastructure and facilities, underscoring the critical importance of considering seismic hazards in landslide susceptibility assessments.

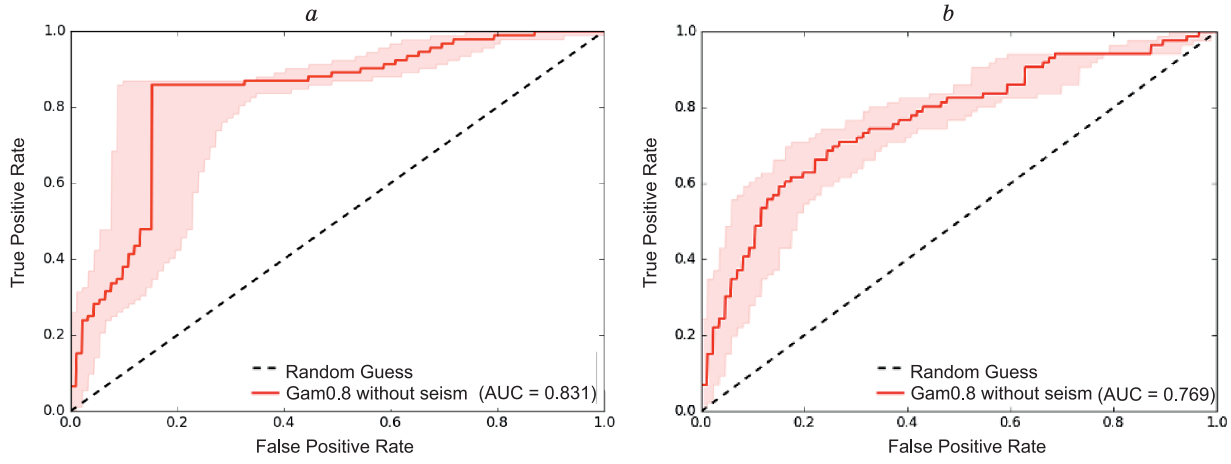

Fig. 16. AUC score. *a* – Including earthquake; *b* – without including earthquake.

The authors are thankful to the civil authorities and inhabitants of El Kherba and Grarem Gouga for their important help in the field. The authors are grateful to the editor and the anonymous reviewer for their useful suggestions and constructive comments, which improved the quality of the manuscript.

This research did not receive any specific grants from funding agencies in the public, commercial, or not-for-profit sectors.

REFERENCES

Abbes, K., Dorbath, C., Dorbath, L., Bouhadad, Y., Ousadou, F., Bezzeghoud, M., 2019. Revisiting the Laalam (Eastern Algeria) March 20, 2006 (M_w 5.1) earthquake and its seismotectonic implication. Pure Appl. Geophys. 176, 4213–4222, doi: 10.1007/s00024-019-02206-3.

Aicha, B., Mezhoud, S., 2021. Numerical modelling of the behavior of tunnel in soft surrounding rock: A case study of Djebel El-Ouahch Tunnel, Algeria. Geotech. Geol. Eng. 39, 5505–5516, doi: 10.21203/rs.3.rs-163604/v1.

Aicha, B., Mezhoud, S., Tayeb, B., Toufik, K., Abdelkader, N., 2022. Parametric study of shallow tunnel under seismic conditions for Constantine motorway tunnel, Algeria. Geotech. Geol. Eng. 40, 2307–2318, doi: 10.1007/s10706-021-02029-x.

Ayadi, A., Bezzeghoud, M., 2015. Seismicity of Algeria from 1365 to 2013: Maximum observed intensity map (MOI2014). Seismol. Res. Lett. 86, 236–244, doi: 10.1785/0220140075.

Bahrami, Y., Hassani, H., Maghsoudi, A., 2021. Landslide susceptibility mapping using AHP and fuzzy methods in the Gilan province, Iran. GeoJournal 86, 1797–1816, doi: 10.1007/s10708-020-10162-y.

Bamutaze, Y., 2019. Morphometric conditions underpinning the spatial and temporal dynamics of landslide hazards on the volcanics of Mt. Elgon, Eastern Uganda, in: Emerging Voices in Natural Hazards Research. Butterworth-Heinemann, doi: 10.1016/B978-0-12-815821-0.00010-2.

Baral, A., Poumand, P., Adhikari, I., Abediniangerabi, B., Shahandashti, M., 2021. A GIS-based data integration approach for rainfall-induced slope failure susceptibility mapping in clayey soils. Nat. Hazards Rev. 22, 04021026, doi: 10.1061/(ASCE)NH.1527-6996.0000478.

Belabbès, S., Wicks, C., Çakir, Z., Meghraoui, M., 2009. Rupture parameters of the 2003 Zemmouri (Mw 6.8), Algeria, earthquake from joint inversion of interferometric synthetic aperture radar, coastal uplift, and GPS. J. Geophys. Res.: Solid Earth 114 (B3), doi: 10.1029/2008JB005912.

Beldjoudi, H., Delouis, B., Djellit, H., Yelles-Chaouche, A., Gharbi, S., Abacha, I., 2016. The Beni-Ilmane (Algeria) seismic sequence of May 2010: Seismic sources and stress tensor calculations. Tectonophysics 670, 101–114, doi: 10.1016/j.tecto.2015.12.021.

Bendjama, H., Yelles-Chaouche, A., Boulahia, O., Abacha, I., Mohammedi, Y., Beldjoudi, H., Rahmani, S.T.E., Belheouane, O., 2021. The March 2017 earthquake sequence along the EW-trending Mcid Aïcha-Debbagh Fault, northeast Algeria. Geosci. J. 25, 697–713, doi: 10.1007/s12303-020-0059-y.

Benfedda, A., Bouhadad, Y., Boughacha, M.S., Guessoum, N., Abbes, K., Bezzeghoud, M., 2020. The Oran January 9th (Mw 4.7) and June 6th, 2008 (Mw 5.4) earthquakes: Seismological study and seismotectonic implication. J. Afr. Earth Sci. 169, 103896, doi: 10.1016/j.jafrearsci.2020.103896.

Benouar, D., 1994. Material for the investigation of the seismicity of Algeria and adjacent regions during the twentieth century. Ann. Geofis. 37, 860, doi: 10.4401/ag-4466.

Berkane, A., Mezhoud, S., Karech, T., Beroual, A., 2022. Numerical analysis of the dynamic behavior of shallow tunnel: A case study of Djebel El-Ouahch tunnel, Algeria. Transp. Infrastruct. Geotechnol. 9, 385–401, doi: 10.1007/s40515-021-00183-6.

Bouhadad, Y., Nour, A., Laouami, N., Belhai, D., 2003. The Beni-Ourtilane-Tachaouaft fault and seismotectonic aspects of the Babors region (NE of Algeria). J. Seismolog. 7, 79–88, doi: 10.1023/A:1021259931865.

Bouhadad, Y., Benhamouche, A., Maouche, S., Belhai, D., 2009. Evidence for Quaternary liquefaction-induced features in the epicentral area of the 21 May 2003 Zemmouri earthquake (Algeria, M_w = 6.8). J. Seismol. 13, 161–172, doi: 10.1007/s10950-008-9134-y.

Bounif, A., Haessler, H., Meghraoui, M., 1987. The Constantine (northeast Algeria) earthquake of October 27, 1985: surface ruptures and aftershock study. Earth Planet. Sci. Lett. 85, 451–460, doi: 10.1016/0012-821X(87)90140-3.

Chandrasekaran, S.S., Senthilkumar, V., Maji, V.B., 2019. Landslides in Nilgiris: causal factors and remedial measures, in: Geotechnical Design and Practice. Springer, Singapore, pp. 183–193, doi: 10.1007/978-981-13-0505-4_16.

Coiffait, P.E., 1992. Un bassin post-nappe dans son cadre structural: l'exemple du bassin de Constantine (Algérie nord-orientale). Doctoral Dissertation, Nancy I.

Conforti, M., Pascale, S., Robustelli, G., Sdao, F., 2014. Evaluation of prediction capability of the artificial neural networks for mapping landslide susceptibility in the Turbolo River catchment (northern Calabria, Italy). Catena 113, 236–250, doi: 10.1016/j.catena.2013.08.006.

Giles, D.P., Griffiths, J.S. (Eds.), 2020. Geological Hazards in the UK: Their Occurrence, Monitoring and Mitigation. Geol. Soc. London.

Grima, N., Edwards, D., Edwards, F., Petley, D., Fisher, B., 2020. Landslides in the Andes: Forests can provide cost-effective landslide regulation services. Sci. Total Environ. 745, 141128, doi: 10.1016/j.scitotenv.2020.141128.

Harbi, A., Maouche, S., Vaccari, F., Aoudia, A., Oussadou, F., Panza, G.F., Benouar, D., 2007. Seismicity, seismic input and site effects in the Sahel—Algiers region (North Algeria). Soil Dyn. Earthquake Eng. 27, 427–447, doi: 10.1016/j.soildyn.2006.10.002.

Kayastha, P., Bijukchhen, S.M., Dhital, M.R., De Smedt, F., 2013. GIS based landslide susceptibility mapping using a fuzzy logic approach: A case study from Ghurmi-Dhad Khola area, Eastern Nepal. J. Geol. Soc. India 82, 249–261, doi: 10.1007/s12594-013-0147-y.

Kherroubi, A., Déverchère, J., Yelles, A., De Lépinay, B.M., Domzig, A., Cattaneo, A., Bracène R., Gaullier V., Graindorge, D., 2009. Recent and active deformation pattern off the easternmost Algerian margin, Western Mediterranean Sea: New evidence for contractional tectonic reactivation. Mar. Geol. 261, 17–32, doi: 10.1016/j.margeo.2008.05.016.

Lee, S., 2007. Application and verification of fuzzy algebraic operators to landslide susceptibility mapping. Environ. Geol. 52, 615–623, doi: 10.1007/s00254-006-0491-y.

Li, R., Wang, N., 2019. Landslide susceptibility mapping for the Muchuan county (China): A comparison between bivariate statistical models (WoE, EBF, and IoE) and their ensembles with logistic regression. Symmetry 11 (6), 762, doi: 10.3390/sym11060762.

Lolli, B., Gasperini, P., Vannucci, G., 2014. Empirical conversion between teleseismic magnitudes (m_b and M_s) and moment magnitude (M_w) at the Global, Euro-Mediterranean and Italian scale. Geophys. J. Int. 199, 805–828, doi: 10.1093/gji/ggu264.

Manchar, N., Hadji, R., Bougherara, A., Boufaa, K., 2022. Assessment of relative-active tectonics in Rhumel-Smendou basin (NE Algeria)–observations from the morphometric indices and hydrographic features obtained by the digital elevation model. Geomatics Land Manage. Landscape 4, 47–65, doi: 10.15576/GLL/2022.4.47.

Mandal, B., Mandal, S., 2018. Analytical hierarchy process (AHP) based landslide susceptibility mapping of Lish river basin of eastern Darjeeling Himalaya, India. Adv. Space Res. 62, 3114–3132, doi: 10.1016/j.asr.2018.08.008.

Meghraoui, M., 1988. Géologie des zones sismiques du Nord de l'Algérie. Paléosismologie, tectonique active et synthèse sismotectonique. Thèse doct. Univ. Paris VI.

Merghadi, A., Abderrahmane, B., Tien Bui, D., 2018. Landslide susceptibility assessment at Mila Basin (Algeria): a comparative assessment of prediction capability of advanced machine learning methods. ISPRS Int. J. Geo-Inf. 7, 268, doi: 10.3390/sym11060762.

Mertens, K., Jacobs, L., Maes, J., Poesen, J., Kervyn, M., Vranken, L., 2018. Disaster risk reduction among households exposed to landslide hazard: A crucial role for self-efficacy? Land Use Policy 75, 77–91, doi: 10.1016/j.landusepol.2018.01.028.

Mezhoud, S., Clastres, P., Houari, H., Belachia, M., 2017. Forensic investigation of causes of premature longitudinal cracking in a newly constructed highway with a composite pavement system. J. Perform. Constr. Facil. 31, 04016095, doi: 10.1061/(ASCE)CF.1943-5509.0000956.

Min, D.H., Yoon, H.K., 2021. Suggestion for a new deterministic model coupled with machine learning techniques for landslide susceptibility mapping. Sci. Rep. 11, 1–24, doi: 10.1038/s41598-021-86137-x.

Mohan, A., Singh, A.K., Kumar, B., Dwivedi, R., 2021. Review on remote sensing methods for landslide detection using machine and deep learning. Trans. Emerging Telecommun. Technol. 32, e3998, doi: 10.1002/ett.3998.

Mouloud, H., Chaker, A., Nassim, H., Lebdioui, S., Rodrigues, H., Agius, M.R., 2023. Post-earthquake damage classification and assessment: case study of the residential buildings after the M_w = 5 earthquake in Mila city, Northeast Algeria on August 7, 2020. Bull. Earthquake Eng. 21, 849–891, doi: 10.21203/rs.3.rs-1803714/v1.

Nosov, M.A., Bolshakova, A.V., 2020. Tsunami Generation by Earthquake. Janus-K, Moscow.

Ordaz, M., Martinelli, F., D'Amico, V., Meletti, C., 2013. CRISIS2008: A flexible tool to perform probabilistic seismic hazard assessment. Seismol. Res. Lett. 84, 495–504, doi: 10.1785/0220120067.

Ortiz, J.A.V., Martínez-Graña, A.M., 2018. A neural network model applied to landslide susceptibility analysis (Capitanejo, Colombia). Geomatics Nat. Hazards Risk 9, 1106–1128, doi: 10.1080/19475705.2018.1513083.

Ousadou, F., Dorbath, L., Dorbath, C., Bounif, M.A., Benhallou, H., 2013. The Constantine (Algeria) seismic sequence of 27 October 1985: a new rupture model from aftershock relocation, focal mechanisms, and stress tensors. J. Seismol. 17, 207–222, doi: 10.1007/s10950-012-9320-9.

Rahali, H., 2019. Improving the reliability of landslide susceptibility mapping through spatial uncertainty analysis: A case study of Al Hoceima, Northern Morocco. Geocarto Int. 34, 43–77, doi: 10.1080/10106049.2017.1357767.

Razifard, M., Shoaei, G., Zare, M., 2019. Application of fuzzy logic in the preparation of hazard maps of landslides triggered by the twin Ahar-Varzeghan earthquakes (2012). Bull. Eng. Geol. Environ. 78, 223–245, doi: 10.1007/s10064-018-1235-4.

Saaty, T.L., 1977. A scaling method for priorities in hierarchical structures. J. Math. Psychol. 15, 234–281, doi: 10.1016/0022-2496(77)90033-5.

Serkhane, A., Benfedda, A., Guettouche, M.S., Bouhadad, Y., 2022. InSAR derived co-seismic deformation triggered by the Mihoub (Tell Atlas of Algeria) 28 May 2016 (Mw = 5.4) earthquake combined to geomorphic features analysis to identify the causative active fault. J. Afr. Earth Sci. 188, 104476, doi: 10.1016/j.jafrearsci.2022.104476.

Shano, L., Raghuvanshi, T.K., Meten, M., 2020. Landslide susceptibility evaluation and hazard zonation techniques – a review. Geoenviron. Disasters 7, 1–19, doi: 10.1186/s40677-020-00152-0.

Swets, J.A., 1988. Measuring the accuracy of diagnostic systems. Science 240, 1285–1293, doi: 10.1126/science.3287615.

Tangestani, M.H., 2004. Landslide susceptibility mapping using the fuzzy gamma approach in a GIS, Kakan catchment area, southwest Iran. Aust. J. Earth Sci. 51, 439–450, doi: 10.1111/j.1400-0952.2004.01068.x.

Tsangaratos, P., Loupasakis, C., Nikolakopoulos, K., Angelitsa, V., Ilia, I., 2018. Developing a landslide susceptibility map based on remote sensing, fuzzy logic and expert knowledge of the Island of Lefkada, Greece. Environ. Earth Sci. 77, 363, doi: 10.1007/s12665-018-7548-6.

Vila, J.M., 1977. Carte géologique de l'Algérie au 1/200,000, feuille de Constantine (PQ; 3-4), avec notice explicative détaillée [Geological Map of Algeria at 1/200,000, Constantine Sheet (PQ; 3-4), with Detailed Explanatory Notes]. Publ. Comm. Serv. Carte Géol. Algérie/SONATRACH, Algeria.

Vila, J.M., 1980. La chaîne alpine de l'Algérie orientale et des confins algéro-tunisiens. Thèse de Doctorat-es-sciences, Univ. Pierre et Marie Curie.

Wallemacq, P., Below, R., McClean, D., 2018. Economic Losses, Poverty and Disasters: 1998–2017. United Nations Office for Disaster Risk Reduction, Geneva.

Wang, Z., Wang, D., Guo, Q., Wang, D., 2020. Regional landslide hazard assessment through integrating susceptibility index and rainfall process. Nat. Hazards 104, 2153–2173, doi: 10.1007/s11069-020-04265-5.

Zadeh, L.A., 1965. Fuzzy sets. Inf. Control 8, 338–353, doi: 10.1016/S0019-9958(65)90241-X.

Zadeh, L.A., Klir, G.J., Yuan, B., 1996. Fuzzy Sets, Fuzzy Logic, and Fuzzy Systems: Selected Papers (Vol. 6). World Scientific.

Zimmermann, H.-J., 1996. Fuzzy Set Theory and Its Applications. 2nd ed. Kluwer, Norwell, MA.